

Proton-proton scattering above 3 GeV/c

A. Sibirtsev^{1,2,3}, J. Haidenbauer^{3,4}, H.-W. Hammer¹, S. Krewald^{3,4} and U.-G. Meißner^{1,3,4}

¹ Helmholtz-Institut für Strahlen- und Kernphysik (Theorie) und Bethe Center for Theoretical Physics, Universität Bonn, D-53115 Bonn, Germany

² Excited Baryon Analysis Center (EBAC), Thomas Jefferson National Accelerator Facility, Newport News, Virginia 23606, USA

³ Institut für Kernphysik and Jülich Center for Hadron Physics, Forschungszentrum Jülich, D-52425 Jülich, Germany

⁴ Institute for Advanced Simulation, Forschungszentrum Jülich, D-52425 Jülich, Germany

Received: date / Revised version: date

Abstract. A large set of data on proton-proton differential cross sections, analyzing powers and the double polarization parameter A_{NN} is analyzed employing the Regge formalism. We find that the data available at proton beam momenta from 3 GeV/c to 50 GeV/c exhibit features that are very well in line with the general characteristics of Regge phenomenology and can be described with a model that includes the ρ , ω , f_2 , and a_2 trajectories and single Pomeron exchange. Additional data, specifically for spin-dependent observables at forward angles, would be very helpful for testing and refining our Regge model.

PACS. 13.75.-n Hadron-induced low- and intermediate energy reactions – 11.55.Jy Regge formalism

1 Introduction

Nucleon-nucleon (NN) elastic scattering is *the* primary process to understand nuclear forces and to construct theoretical models of the strong interaction. While relativistic meson-exchange models [1, 2, 3, 4, 5, 6, 7, 8, 9, 10, 11, 12] work reasonably well at beam momenta below 2 GeV/c, say, the situation is quite different at higher proton momenta. The typical problems are summarized in Refs. [11, 13]. First, the predicted NN elastic cross sections are too large and increase with momentum, while experimentally they decrease. Second, the predicted analyzing powers are too large while for other spin observables even the sign differs from that observed in experiments. The first problem is caused by the vector-meson exchange in the standard meson-exchange models. It was claimed [13] that, because of the first problem, Regge theory was invented since it generates the appropriate energy dependence of the scattering amplitude. The second problem, however, persists even when the contribution from vector mesons is taken off. Thus, the momentum range from 2 GeV/c to 10 GeV/c offers precise and still unexplained data, waiting for being described by adequate models.

During the last years some progress was achieved in the analysis of NN scattering below $\simeq 4$ GeV/c within an approach based on relativistic optical potentials [14, 15, 16, 17]. Other recent activities concern the application of the Regge formalism [18, 19, 20, 21, 22] in the analysis of proton-proton (pp) scattering at very high momenta, say above 100 GeV/c. Here the most interesting finding is

that there are possibly contributions from new Pomeron trajectories [22, 23] that are insignificant at low energies.

The most recent extensive measurements of pp scattering were done by the EDDA Collaboration at COSY [24, 25] and at SATURNE in Saclay [26, 27, 28, 29, 30]. These experiments provide a wealth of precise data on differential cross sections and polarizations up to beam momenta of about 3.8 GeV/c. Unfortunately, these measurements do not cover forward angles below $\theta_{c.m.} \simeq 30^\circ$. A further improvement of the high-quality data base on pp scattering is expected from the ANKE Collaboration at COSY. Very recently it was proposed [31] to measure pp elastic scattering at beam momenta from 2.4 GeV/c to 3.6 GeV/c and at c.m. angles from 10° to 30° . The experiment aims to obtain precision data for differential cross sections and analyzing powers. The experiment could be extended in the future to measure double polarization observables.

The findings in Refs. [11, 13] show that traditional nuclear models of the NN interaction such as meson-exchange potentials cannot be easily extended to the energies covered by the COSY-EDDA and SATURNE experiments. At the same time that region is much too low for perturbative QCD to be applied. Thus, in this paper we propose to use a phenomenological Regge approach to study the NN interaction at those COSY-EDDA and SATURNE energies.

In the present paper we consider the ρ , ω , f_2 , and a_2 Regge exchanges, supplemented by the contribution of a single Pomeron Regge pole. We expect that those conventional Regge trajectories represent the proper dynamical degrees of freedom for describing NN scattering in the

region from the COSY-EDDA and SATURNE energies up to beam momenta of 50 to 100 GeV/c. Indeed at the latter momenta the pp and antiproton-proton ($\bar{p}p$) cross sections are already pretty close to each other, cf. the review section of the PDG [32], which is a clear indication that the contributions from the mesonic Regge trajectories have become practically negligible and pp (as well as $\bar{p}p$) scattering is dominated by Pomeron exchange alone. In fact, as already said above, at such high momenta additional dynamical mechanisms become more and more important which do not play a role for energies down to the COSY-EDDA and SATURNE regime.

As will be shown in this paper, with contributions from the ρ , ω , f_2 , and a_2 Regge exchanges and a single Pomeron Regge pole we are able to describe the pp , $\bar{p}p$, pn , $\bar{p}n$ total cross sections, but also the ratio of the real-to-imaginary parts of the forward amplitudes for pp and $\bar{p}p$, over a large energy range up to beam momenta of around 100 GeV/c. Next, we use the data on angular distributions and polarizations for pp to determine the details of the Regge exchanges. Obviously, it is an open question down to which energies such a phenomenological Regge approach can provide a quantitative description of the available data. We find that the phenomenology allows to achieve a useful representation of the data down to 3 GeV/c, in line with analogous investigations for pion-nucleon scattering [33,34,35,36,37]. The Regge region therefore turns out to have a significant overlap with the kinematical region covered by the COSY-EDDA and SATURNE pp experiments.

The paper is organized as follows: In sect. 2, we introduce the helicity amplitudes for pp scattering. In sect. 3 we describe the details of the fitting procedure. Sect. 4 provides a comparison of the results of our Regge model with data on differential cross sections and polarizations. In sect. 5 a comparison between the Regge calculation and results based on the partial wave analysis (PWA) of the George-Washington Group (GWU) is made for some beam momenta. The paper ends with a summary. Detailed information on the data sets used in our analysis are summarized in an Appendix.

2 Helicity amplitudes

In the past Regge analyses of NN scattering at beam momenta from 3 GeV/c upwards were presented in Refs. [38, 39]. Unfortunately, the proposed formalism cannot be simply taken over for the study of the new data. In Ref. [38] the amplitudes are expanded for very low momentum transfer squared or for very forward angles. The analysis of Ref. [39] is fairly complete but, strictly speaking, is not based on a covariant formulation. For instance the Regge propagator is expressed not in terms of Mandelstam invariants like the squared invariant collision energy s , as usually done, but in terms of the laboratory energy. This is in conflict with the energy dependence of the total pp cross section, where there is strong evidence [40,41] that its s -dependence is driven by the leading Regge trajectories.

It is convenient to expand the NN scattering matrix ϕ in terms of the helicity amplitudes proposed by Jacob and Wick [42]:

$$\phi_a = \langle \lambda'_1 \lambda'_2 | \phi | \lambda_1 \lambda_2 \rangle, \quad (1)$$

Here $\lambda_1(\lambda'_1)$ and $\lambda_2(\lambda'_2)$ are the s -channel projections of the spin of the initial (final) protons, respectively. The index a labels all possible combinations of helicities for the transition between initial and final states. Taking into account parity conservation and time reversal invariance [43] the full set of the covariant s -channel helicity amplitudes is given by [44]

$$\begin{aligned} \phi_1 &= \langle +\frac{1}{2} +\frac{1}{2} | \phi | +\frac{1}{2} +\frac{1}{2} \rangle = \langle -\frac{1}{2} -\frac{1}{2} | \phi | -\frac{1}{2} -\frac{1}{2} \rangle, \\ \phi_2 &= \langle +\frac{1}{2} +\frac{1}{2} | \phi | -\frac{1}{2} -\frac{1}{2} \rangle = \langle -\frac{1}{2} -\frac{1}{2} | \phi | +\frac{1}{2} +\frac{1}{2} \rangle, \\ \phi_3 &= \langle +\frac{1}{2} -\frac{1}{2} | \phi | +\frac{1}{2} -\frac{1}{2} \rangle = \langle -\frac{1}{2} +\frac{1}{2} | \phi | -\frac{1}{2} +\frac{1}{2} \rangle, \\ \phi_4 &= \langle +\frac{1}{2} -\frac{1}{2} | \phi | -\frac{1}{2} +\frac{1}{2} \rangle = \langle -\frac{1}{2} +\frac{1}{2} | \phi | +\frac{1}{2} -\frac{1}{2} \rangle, \\ \phi_5 &= \langle +\frac{1}{2} +\frac{1}{2} | \phi | +\frac{1}{2} -\frac{1}{2} \rangle = \langle -\frac{1}{2} +\frac{1}{2} | \phi | -\frac{1}{2} -\frac{1}{2} \rangle \\ &= \langle -\frac{1}{2} -\frac{1}{2} | \phi | +\frac{1}{2} -\frac{1}{2} \rangle = \langle -\frac{1}{2} +\frac{1}{2} | \phi | +\frac{1}{2} +\frac{1}{2} \rangle \\ &= -\langle -\frac{1}{2} -\frac{1}{2} | \phi | -\frac{1}{2} +\frac{1}{2} \rangle = -\langle +\frac{1}{2} -\frac{1}{2} | \phi | +\frac{1}{2} +\frac{1}{2} \rangle \\ &= -\langle +\frac{1}{2} +\frac{1}{2} | \phi | -\frac{1}{2} +\frac{1}{2} \rangle = -\langle +\frac{1}{2} -\frac{1}{2} | \phi | -\frac{1}{2} -\frac{1}{2} \rangle. \end{aligned} \quad (2)$$

Therefore, elastic scattering of two identical particles with spin-1/2 can be completely described by five independent amplitudes. The helicity amplitudes ϕ_1 and ϕ_3 given above correspond to helicity nonflip, ϕ_5 is the single helicity-flip amplitude, while ϕ_2 and ϕ_4 are double helicity-flip amplitudes.

The helicity amplitudes depend on the invariant kinematic variables defined as

$$\begin{aligned} s &= (p_1 + p_2)^2 = (p'_1 + p'_2)^2, \\ t &= (p_1 - p'_1)^2 = (p_2 - p'_2)^2, \\ u &= (p_1 - p'_2)^2 = (p'_1 - p_2)^2, \end{aligned} \quad (3)$$

where p_1 (p'_1) and p_2 (p'_2) are the four-momenta of the incident (final) protons, respectively, and

$$s + t + u = 4m_N^2, \quad (4)$$

with m_N being the proton mass.

We consider pp scattering via the exchange of Regge trajectories defined by a certain set of allowed quantum numbers. Within the Regge formalism the helicity amplitudes ϕ_a ($a=1, \dots, 5$) can be parameterized for each exchange trajectory i by

$$\phi_{ai}(s, t) = \pi \beta_{ai}(t) \frac{\zeta_i(s, t)}{\Gamma(\alpha(t))}, \quad (5)$$

where β_{ai} is the product of the vertex functions and Γ denotes the Γ -function that is introduced in order to suppress the poles of the Regge propagator in the scattering region. The total helicity amplitudes are given by the

corresponding sum over the contributing trajectories. Furthermore, ζ_i is the Regge propagator taken to be

$$\zeta_i(t, s) = \frac{1 + \mathcal{S}_i \exp[-i\pi\alpha_i(t)]}{\sin[\pi\alpha_i(t)]} \left[\frac{s}{s_0} \right]^{\alpha_i(t)}, \quad (6)$$

with \mathcal{S}_i being the signature of the trajectory and $s_0 = 1 \text{ GeV}^2$ a scaling factor. The i -th Regge trajectory, α_i , is considered as a linear function of t ,

$$\alpha_i(t) = \alpha_i^0 + \alpha_i' t, \quad (7)$$

with the slope α_i' and the intercept α_i^0 either being determined by a fit to data or taken from the analysis of other reactions. Note that the difference between the power $\alpha(t)$ here and the power $\alpha(t)-1$ given in our previous publications [33,35,36] on meson photoproduction and pion charge-exchange is due to different normalizations, *i. e.* different relations between the helicity amplitudes and observables.

The signature \mathcal{S}_i of the exchange trajectory is defined as follows. Both natural and unnatural parity trajectories can be exchanged in the t -channel. The naturalness \mathcal{N} for natural ($\mathcal{N}=+1$) and unnatural ($\mathcal{N}=-1$) parity exchanges is defined as

$$\begin{aligned} \mathcal{N} &= +1 \text{ if } P = (-1)^J, \\ \mathcal{N} &= -1 \text{ if } P = (-1)^{J+1}, \end{aligned} \quad (8)$$

where P and J are the parity and spin of the particle lying on the Regge trajectory. The signature factor $\mathcal{S}=\pm 1$ is then defined as [45,46,47]

$$\mathcal{S} = P \times \mathcal{N} = (-1)^J. \quad (9)$$

The structure of the functions β_{ai} of Eq. (5) is defined by the quantum numbers of the particles at the interaction vertices, similar to the usual particle-exchange Feynman diagram. The general form of the functions β_{ai} is given by [45]

$$\beta_{ai}(t) = c_{ai} F_{ai}(t) \left[\frac{-t}{4m_N^2} \right]^{\frac{|\lambda_1' - \lambda_1|}{2}} \left[\frac{-t}{4m_N^2} \right]^{\frac{|\lambda_2' - \lambda_2|}{2}}, \quad (10)$$

where c_{ai} is a constant and F_{ai} is an overall form factor. For the latter we take an exponential function so that in our case the β_{ai} are parameterized by

$$\begin{aligned} \beta_{1i}(t) &= c_{1i} \exp(b_{1i}t), \\ \beta_{2i}(t) &= c_{2i} \exp(b_{2i}t) \frac{-t}{4m_N^2}, \\ \beta_{3i}(t) &= c_{3i} \exp(b_{3i}t), \\ \beta_{4i}(t) &= c_{4i} \exp(b_{4i}t) \frac{-t}{4m_N^2}, \\ \beta_{5i}(t) &= c_{5i} \exp(b_{5i}t) \left[\frac{-t}{4m_N^2} \right]^{1/2}. \end{aligned} \quad (11)$$

Therefore, in general for each trajectory that contributes to pp elastic scattering one should determine 10 free parameters, in case that the intercepts and slopes of the trajectories are known from other sources.

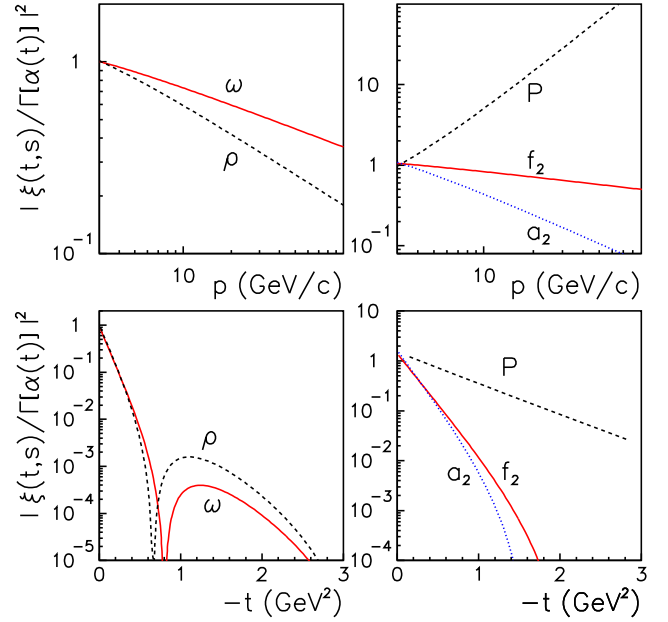


Fig. 1. Absolute square of the Regge propagator of Eq. (6) divided by the Γ -function as a function of the beam momentum (upper panel) at fixed $t=-1 \text{ GeV}^2$ and as a function of the four-momentum transfer squared (lower panel) at the beam momentum $p=5 \text{ GeV/c}$. Results are presented for the ρ , ω , f_2 , a_2 , and Pomeron (P) trajectories as indicated in the plots.

In the asymptotic limit, *i. e.* for large s and small $|t|$, the helicity amplitudes exhibit the property [48,49]

$$\phi_{1i} = \phi_{3i} \quad \text{and} \quad \phi_{2i} = -\phi_{4i}. \quad (12)$$

This allows to reduce the number of free parameters to six for each trajectory. However, that relation should be considered as a leading order approximation and further improvements of the model might be achieved by considering not only three but the complete set of five independent amplitudes as given by Eq. (11). Nevertheless, we try to keep the number of free parameters as small as possible, because the amount of polarization data, to which the calculations are very sensitive, is rather limited at high energies.

Let us now specify the trajectories that contribute to pp scattering. At high energies hadron-hadron scattering is dominated by Pomeron exchange. We consider here a single Pomeron Regge pole for which we adopt the parameters [50,51,52]

$$\alpha_P(t) = 1.08 + 0.25t. \quad (13)$$

The ρ and ω trajectories are taken from our global analysis of pion charge-exchange [35] and neutral pion photoproduction [36] data. Note that these analyses include experimental results on differential cross sections and on single as well as double polarizations. We take

$$\begin{aligned} \alpha_\rho(t) &= 0.53 + 0.8t, \\ \alpha_\omega(t) &= 0.64 + 0.8t. \end{aligned} \quad (14)$$

For the f_2 and a_2 trajectories we adopt the values from Ref. [53]:

$$\alpha_{f_2}(t) = 0.71 + 0.83t, \quad (15)$$

$$\alpha_{a_2}(t) = 0.45 + 0.91t, \quad (16)$$

These authors fixed the trajectories from a systematic analysis of the mesonic states in the Chew-Frautschi plot, given by the plane defined by the squared mass and the spin of the particles.

Pion exchange plays a significant role at low energies. Specifically, it constitutes the longest ranged part of the pp interaction and it dominates at very small $-t$, i.e. close to the pole of the pion propagator. Indeed, it was argued [59] that the pion pole term dominates so strongly in forward direction, that one can actually extract the πNN coupling constant from the differential cross section by an extrapolation to the pion pole. In the Regge model the pion trajectory is given by [53,54]

$$\alpha_\pi(t) = 0.7(t - m_\pi^2), \quad (17)$$

where m_π is the pion mass. Hence the contribution from pion exchange decreases much more rapidly with increasing beam momentum compared to those of the other contributions and, therefore, is difficult to determine. This problem in determining the contribution from the pion exchange trajectory is further intensified by the lack of pp scattering data in the forward direction at the lower energies considered in the present investigation. Thus, at this stage we do not include the pion trajectory.

It is instructive to look at the beam-momentum- and t dependence for each of the included trajectories. Fig. 1 illustrates the absolute squared Regge propagator of Eq. (6) divided by the Γ -function, *i. e.* $|\zeta_i(t, s)/\Gamma[\alpha_i(t)]|^2$ for different trajectories. The upper panel of Fig. 1 shows the dependence on the laboratory momentum at fixed $t = -1 \text{ GeV}^2$. The results for different trajectories are arbitrarily normalized at $p = 3 \text{ GeV}/c$. It is clear that with increasing momentum, the Pomeron trajectory becomes more and more significant.

The lower panel of Fig. 1 illustrates the t -dependence of $|\zeta_i(t, s)/\Gamma[\alpha_i(t)]|^2$ at the beam momentum $p = 5 \text{ GeV}/c$. The zeros of the amplitudes due to the ρ and ω trajectories are close to each other, but not at exactly the same t . If one of the trajectories dominates the reaction we would expect that there is a minimum in the differential cross section at a certain value of t . Indeed the data on the $\gamma p \rightarrow \pi^0 p$ and $\pi^- p \rightarrow \pi^0 n$ reactions show minima around $-t = 0.5 - 0.6 \text{ GeV}^2$. The minimum could be shifted due to an interference between different trajectories. Moreover, it is possible that the minimum is not observed at all, if the contributing trajectories play an equally important role, like in the $\gamma p \rightarrow \pi^+ n$ and $\gamma n \rightarrow \pi^- p$ reactions.

For scattering of identical particles the amplitudes ϕ_a ($a = 1, \dots, 5$) obey certain symmetry relations. Specifically, for pp scattering they read [43]: $\phi_{1,2}(\theta_{c.m.}) = \phi_{1,2}(\pi - \theta_{c.m.})$, $\phi_3(\theta_{c.m.}) = -\phi_4(\pi - \theta_{c.m.})$, $\phi_5(\theta_{c.m.}) = -\phi_5(\pi - \theta_{c.m.})$. We implement these symmetry relations via the substitution $\phi_1(t) \rightarrow \phi_1(t) + \phi_1(u)$, etc. [55]. This replace-

Table 1. Parameters of the model. The constants c_{ai} are given in $\text{GeV} \cdot \sqrt{mb}$ and the b_{ai} 's are given in GeV^{-2} .

	i	c_{1i}	c_{2i}	c_{5i}
P	1	-10.9 ± 2.3	524 ± 41	-0.98 ± 0.15
f_2	2	-19.0 ± 1.3	-1699 ± 170	322 ± 4
ω	3	11.7 ± 1.2	376 ± 47	-26.5 ± 11.2
ρ	4	2.6 ± 0.3	-216 ± 60	50.3 ± 7.1
a_2	5	-2.8 ± 0.2	1314 ± 390	107.5 ± 12.1

	i	b_{1i}	b_{2i}	b_{5i}
P	1	3.8 ± 0.14	7.45 ± 0.42	2.67 ± 0.25
f_2	2	18.5 ± 6.1	4.2 ± 0.9	21.7 ± 3.2
ω	3	0.28 ± 0.05	0.12 ± 0.04	0.0016 ± 0.00003
ρ	4	36 ± 8	0.0007 ± 0.0003	0.14 ± 0.03
a_2	5	0.57 ± 0.06	1.66 ± 0.23	1.42 ± 0.13

ment has no influence on the results for small $-t$. However, it modifies the amplitudes for t values corresponding to angles close to $\theta_{c.m.} = 90^\circ$. In particular, then the analyzing power vanishes at 90° , as it must be the case for pp scattering.

Finally, the helicity amplitudes are normalized in such a way that the differential cross section is given by

$$\frac{d\sigma}{dt} = \frac{1}{64\pi q^2 s} \frac{1}{2} [|\phi_1|^2 + |\phi_2|^2 + |\phi_3|^2 + |\phi_4|^2 + 4|\phi_5|^2]. \quad (18)$$

The analyzing power A is then given by

$$A \propto -\text{Im}[(\phi_1 + \phi_2 + \phi_3 - \phi_4)\phi_5^*]. \quad (19)$$

A complete overview of the relations between the helicity amplitudes and various observables can be found in Ref. [43].

3 Fit procedure

In our global analysis of the pp scattering data we include five trajectories, namely the Regge amplitudes for ω , ρ , f_2 , a_2 exchanges and the Pomeron. In order to minimize the number of free parameters we impose the asymptotic relations given in Eq. (12). Therefore, there are 30 parameters that have to be determined in a fit to data in order to fix the coupling constants and form factors of Eq. (11). The parameters of the model are compiled in Table 1.

We use data at proton laboratory momenta within the range of 3 to 50 GeV/c (corresponding to invariant collision energies of $2.77 < \sqrt{s} < 10 \text{ GeV}$) because in this region the contributions from the ω , ρ , f_2 and a_2 Regge exchanges play an essential role. As is illustrated in Fig. 1 at higher energies the contributions from those Regge trajectories become almost negligible and pp scattering is dominated by single Pomeron exchange. Indeed at higher collision energies other dynamical mechanisms become very important which, at the same time, are irrelevant in the energy range indicated above. For example, two classes of

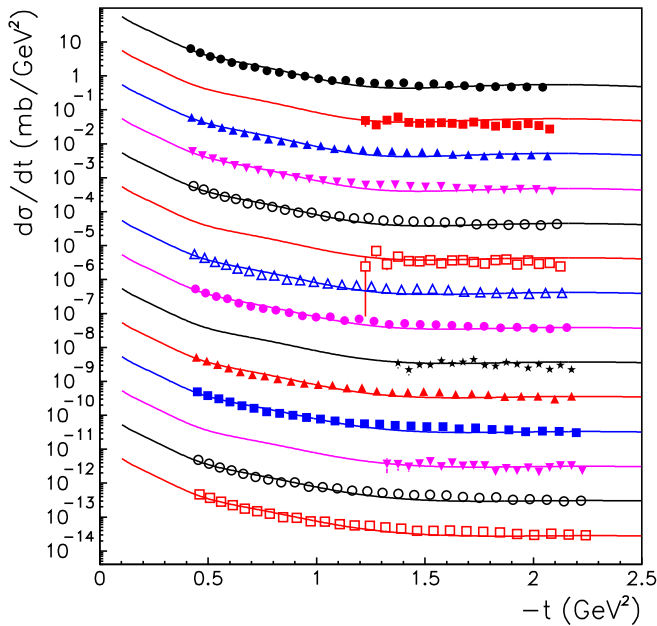


Fig. 2. Differential cross section for pp elastic scattering as a function of the four-momentum transfer squared t . Results are shown for different beam momenta (from top to bottom: 3.012, 3.017, 3.036, 3.062, 3.087, 3.095, 3.112, 3.137, 3.15, 3.162, 3.187, 3.205, 3.212 and 3.237 GeV/c). The solid lines are our model results. The data points and the lines are scaled by factors of 10^0 (top) to 10^{-13} (bottom), consecutively. References to the data are given in Table 2.

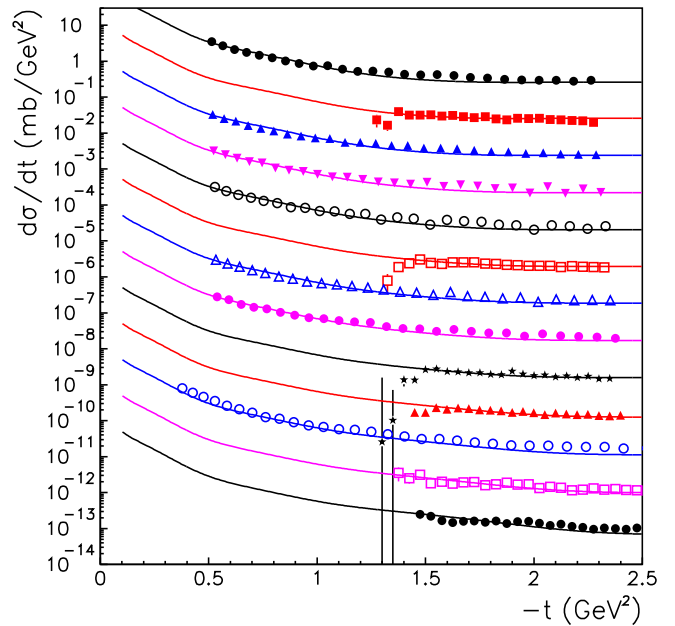


Fig. 3. Differential cross section for pp elastic scattering as a function of the four-momentum transfer squared t . Results are shown for different beam momenta (from top to bottom: 3.262, 3.266, 3.287, 3.312, 3.337, 3.35, 3.362, 3.388, 3.41, 3.469, 3.499, 3.53, 3.621 GeV/c). The solid lines are our model results. The data points and the lines are scaled by factors of 10^0 (top) to 10^{-11} (bottom), consecutively. References to the data are given in Table 2.

Pomeron trajectories are introduced in [21,22,23], namely a soft Pomeron and a hard Pomeron. Other investigations of pp scattering consider also additional contributions [50, 51,56,57] besides the single Pomeron Regge pole, in order to explain the data on differential cross sections at momenta above $\simeq 50$ GeV/c such as double-Pomeron exchange, three-gluon exchange, etc. See also Ref. [58]. Since we are predominantly interested in fixing the contributions from the mentioned well-established traditional Reggeon contributions we do not extend our analysis to such very high energies. In the energy region considered by us a single Pomeron Regge pole is sufficient.

It is not clear a priori down to which energies the Regge formalism is applicable. Our previous systematic analyses of neutral and charged pion photoproduction [34,36,54], on pion charge-exchange [35] and pion-nucleon backward scattering [37] demonstrate that Regge models allow to describe differential cross sections as well as single and double polarization data fairly well down to $p \simeq 3$ GeV/c. Thus, we decided to include in our fit also pp scattering data down to $p \simeq 3$ GeV/c.

Information about the data considered in the present analysis is summarized in an Appendix. There we indicate the beam momenta, the maximal and minimal values of the four-momentum transfer squared, the group who performed the experiment and provide the reference of the publication. We include data in the range $|t| \leq 2.5$ GeV²

which is the range where most of the experiments were performed.

In addition to the data listed in the Appendix we fit the total pp cross section for momenta between 3 and 50 GeV/c and the ratio of the real to imaginary parts of the forward scattering amplitude. Applying the optical theorem this allows us to fix the helicity non-flip amplitude at forward direction, *i. e.* at $t=0$. Moreover, in order to further constrain our amplitudes (but also to test them) we include data on total cross sections for the $\bar{p}p$, pn and $\bar{p}p$ reactions too.

4 Results

4.1 Differential cross sections

In Figs. 2-7 we show data on pp scattering differential cross sections at various beam momenta as indicated in the figures. References to the data are given in Tables 2 and 3. Most of the experimental results in the indicated kinematic region are available from the Zero Gradient Synchrotron (ZGS) at Argonne National Laboratory and from the EDDA Collaboration at COSY in Jülich. The results of our Regge model presented in Figs. 2-6 are based on the central values of the parameters given in Table 1. We do not display here the variations induced by the uncertain-

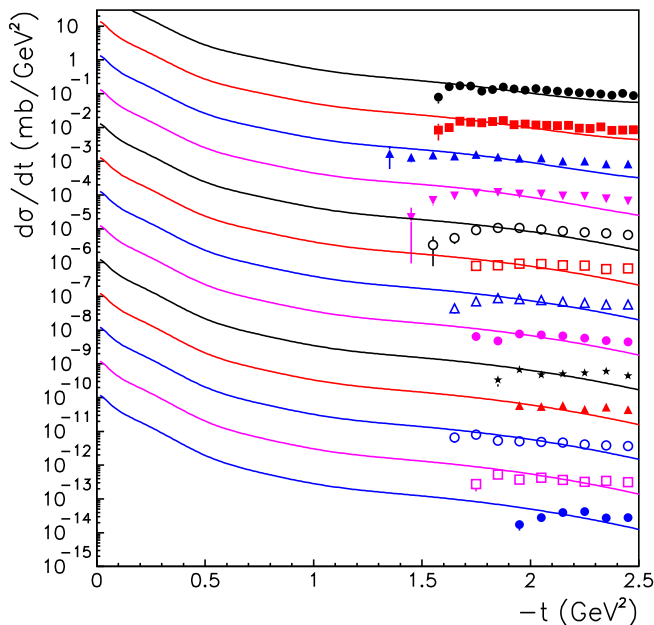


Fig. 4. Differential cross section for pp elastic scattering as a function of the four-momentum transfer squared t . Results are shown for different beam momenta (from top to bottom: 3.686, 3.75, 3.843, 3.942, 4.013, 4.082, 4.151, 4.258, 4.334, 4.409, 4.483, 4.559 and 4.681 GeV/c). The solid lines are our model results. The data points and the lines are scaled by factors of 10^0 (top) to 10^{-12} (bottom), consecutively. References to the data are given in Table 2.

ties in those parameters which are in the order of 20 %, cf. Table 1, in order to avoid too busy figures¹.

Obviously our Regge model yields a good overall reproduction of the differential cross sections over a wide energy range. In particular, it is possible to reproduce the experimental information for beam momenta from 3 to 50 GeV/c with the same set of parameters. The obtained χ^2 is with 1.69 per data point fairly good. Still there is, in average, a discrepancy of about 20% between our model results and some of the data, especially at the lower energies considered. It is partly due to the known disagreement between some differential-cross-section data caused by differences in the absolute cross section normalization of various experiments, discussed in Ref. [61]. As mentioned in this reference, the ZGS ANL results [62,63] are lower by about 20% with respect to the most recent COSY-EDDA data [61] and they also clearly disagree with previous measurements from ZGS ANL [65]. In this context let us also mention that close to the maximal value of the squared four-momentum transfer t accessible at the ZGS ANL experiment some of the differential cross section data deviate significantly from our calculations and seem to indicate an unexpected t -dependence, cf. Figs. 3-4.

¹ Note that more digits are needed for the parameter c_2 for the ω and ρ exchange trajectories if one wants to reproduce our results as given in Figs. 2-6 accurately, namely $c_{2\omega} = 376.117$ and $c_{2\rho} = -216.879$.

The differential cross sections do not show any minima or other structures that correspond to the zeros of the amplitudes due to exchanges of individual trajectories as they are illustrated in Fig. 1. However, at the higher energies considered one can see the onset of a shoulder around $t \approx -1.4$ GeV² (Figs. 5-6) which for very high energies evolves into a dip structure, cf. Refs. [50,51,56,57]. Note that the more pronounced shoulder seen in the measurement at $p=44.5$ GeV/c [91], seems to be in conflict with the bulk of the data as pointed out by E. Martynov [57].

As is clear from the data presented in Figs. 2-3, for momenta between 3 and 3.4 GeV/c there are almost no cross-section data available at $|t| < 0.5$ GeV². Furthermore, in the momentum range $3.5 \leq p < 4.2$ GeV/c there is basically no experimental information at $|t| < 1.5$ GeV². Therefore, our amplitude in forward direction is fixed practically only by the data available at high momenta. Some data at higher momenta and at very-forward angles are displayed in Fig. 7. Obviously, they are all very nicely reproduced by our Regge model. Note that here the contribution of the Coulomb amplitude [64], properly symmetrized, is included in the calculation.

We expect that additional data at small $|t|$ will put more constraints on our solution and, therefore, would allow to determine better the reaction amplitude. Hence, the upcoming data on differential cross sections from ANKE at COSY could play a decisive role for improving the anal-

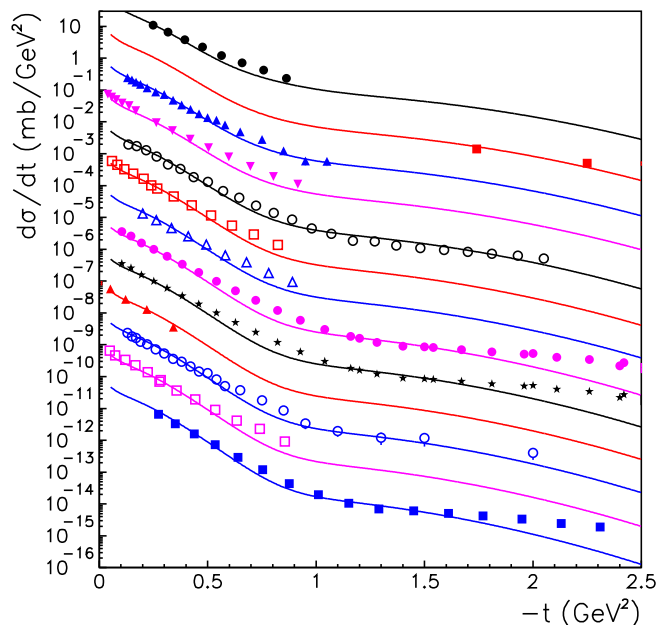


Fig. 5. Differential cross section for pp elastic scattering as a function of the four-momentum transfer squared t . Results are shown for different beam momenta (from top to bottom: 6.8, 8.0, 8.5, 8.8, 10.0, 10.8, 10.94, 12.0, 12.0, 12.1, 12.4, 12.8, 14.2 GeV/c). The solid lines are our model results. The data points and the lines are scaled by factors of 10^0 (top) to 10^{-13} (bottom), consecutively. References to the data are given in Tables 2 and 3.

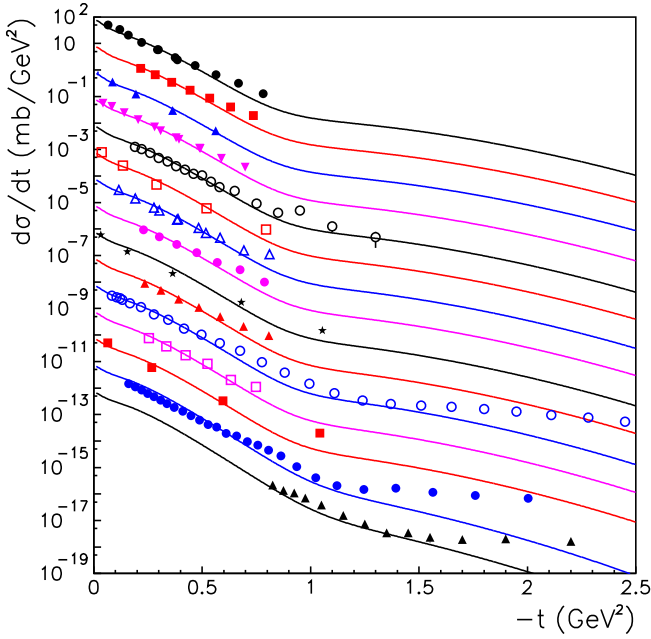


Fig. 6. Differential cross section for pp elastic scattering as a function of the four-momentum transfer squared t . Results are shown for different beam momenta (from top to bottom: 14.8, 14.93, 15.5, 16.7, 18.4, 18.6, 19.6, 19.84, 21.4, 21.88, 24.0, 24.63, 26.2, 44.5, 50.0 GeV/c). The solid lines are our model results. The data points and the lines are scaled by factors of 10^0 (top) to 10^{-13} (bottom), consecutively. References to the data are given in Tables 2 and 3.

ysis and for the extraction of high quality pp scattering amplitudes. As will be discussed in the next section, also the amount of polarization data for low $-t$ is rather limited.

4.2 Analyzing powers

In the following we use the notation given in Table 2 of Bystricky *et al.* [43] for the polarization observables. Furthermore, we assume that $A=P$ which follows from time reversal invariance and we do not specify explicitly which of those two observables was determined in the actual experiment. In the discussion below we refer to the proton polarization data always as analyzing powers.

During the last years an extensive program on measuring analyzing powers for pp elastic scattering was conducted at COSY-EDDA and at SATURNE. At the COSY facility data were taken [24,25] at beam momenta from 1 to 3.3 GeV/c and for scattering angles from 30° to 90° . At SATURNE the measurements were done [27,28] at beam momenta from 2.57 to 3.61 GeV/c and for proton scattering angles typically from 60° to 100° . In addition, within this momentum range there are analyzing powers available from ZGS ANL [62,63]. At higher momenta data are available from ZGS ANL, CERN PS, FNAL, and AGS BNL. References to the data are collected in Table 4.

Figs. 8-11 display pp analyzing powers as a function of the four-momentum transfer squared for different beam

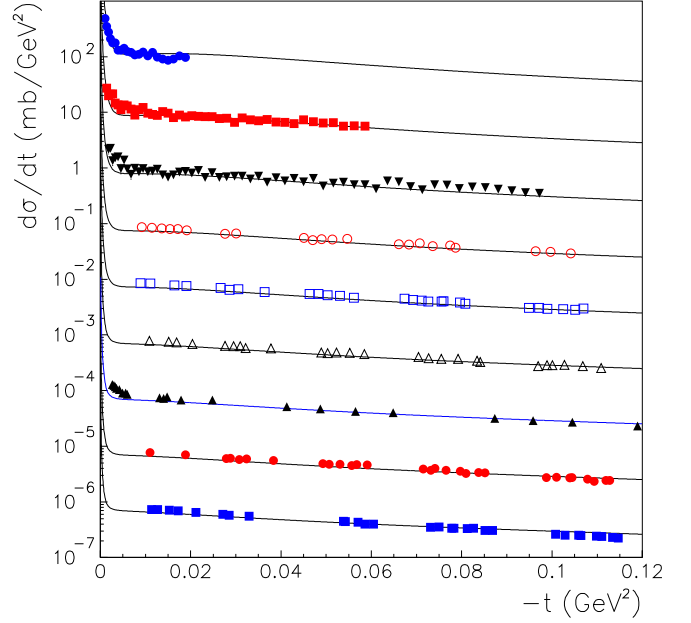


Fig. 7. Differential cross section for pp elastic scattering as a function of the four-momentum transfer squared t . Results are shown for different beam momenta (from top to bottom: 4.2, 7.0, 10.0, 13.16, 15.52, 24.56, 30.0, 30.45, and 45.17 GeV/c). The solid lines are our model results. The data points and the lines are scaled by factors of 10^0 (top) to 10^{-2} (bottom), consecutively. References to the data are given in Tables 2 and 3.

momenta. The symbols indicate the experimental results from different measurements as explained in the figure captions. The data are shown only with statistical errors. The shaded bands illustrate the uncertainties of our calculation. Those bands are obtained by varying the values of the model parameters individually within the one standard deviation given in Table 1. The arrows indicate those values of t which correspond to the pp scattering angle of $\theta_{c.m.} = 90^\circ$. There the analyzing powers equal to zero.

Although the COSY-EDDA and SATURNE measurements provide many precise data these experiments do not cover forward angles and, therefore, the behavior of the amplitudes for scattering angles below 30° is not well constrained experimentally.

The Regge calculation produces a minimum structure in the analyzing power around $-t \simeq 0.5 \div 1$ GeV². The COSY-EDDA [24,25] and ZGS ANL [62,63] data available in that region seem to support such a structure. But there are some beam momenta where the COSY data do not really exhibit a minimum.

It is interesting that the analyzing powers do not vanish at high momenta. Indeed, the data as well as our calculation exhibit some structure. The CERN PS data [74] at the beam momentum of 10 GeV/c (cf. Fig. 11) indicate a distinct maximum of the analyzing power around $-t \simeq 1.6$ GeV². Our Regge model does not produce such a pronounced structure. Other data available at near-by

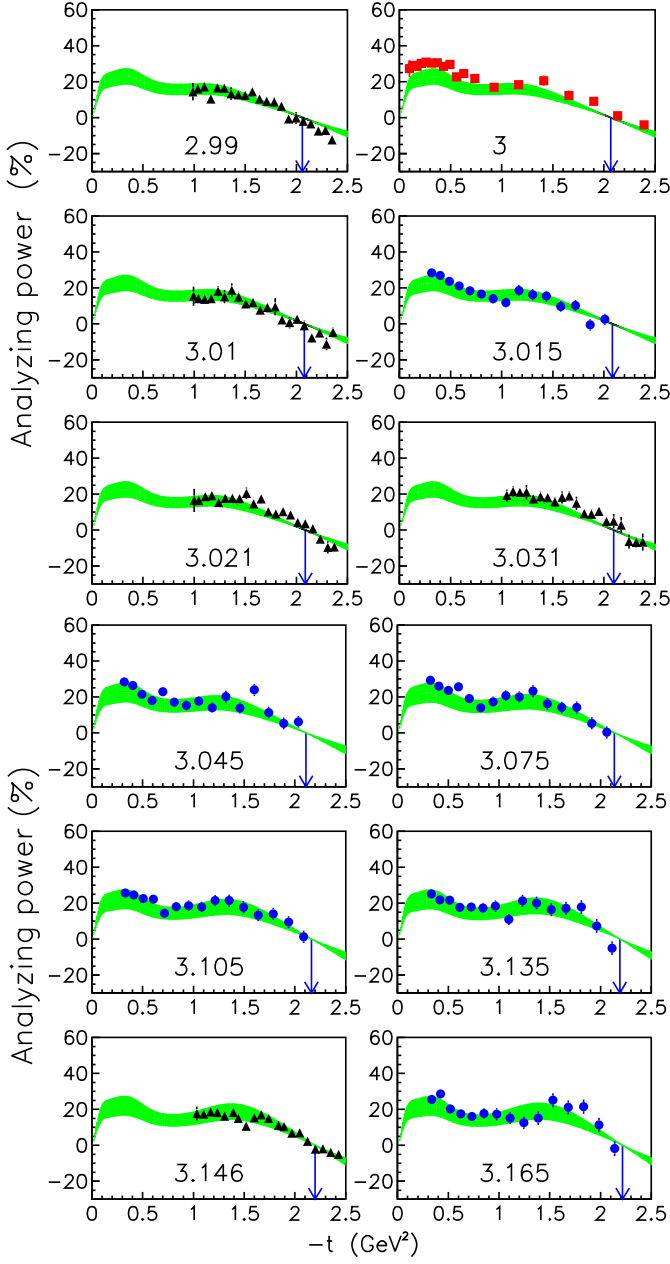


Fig. 8. Analyzing power for pp elastic scattering as a function of the four-momentum transfer squared t for different beam momenta (in GeV/c) as indicated in the figure. The triangles are data from SATURNE [27,28], the squares are from ZGS ANL [66], and the circles are from COSY-EDDA [24,25]. The shaded bands illustrate the uncertainty of our calculation. The arrows indicate the squared four-momenta corresponding to the scattering angle $\theta_{c.m.}=90^\circ$.

beam momenta do not show such a pronounced structure either.

4.3 Double polarization parameter A_{NN}

The double polarization parameters discussed here can be measured with a vertically polarized beam and a vertically

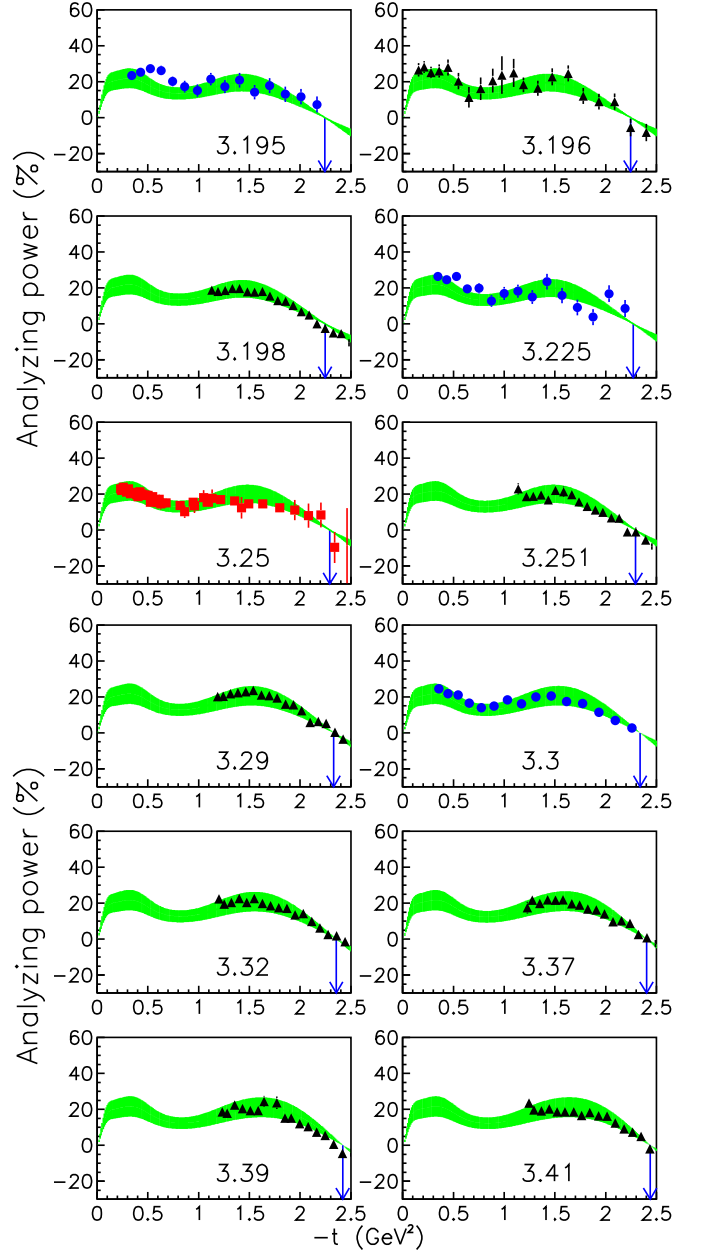


Fig. 9. Analyzing power for pp elastic scattering as a function of the four-momentum transfer squared t for different beam momenta (in GeV/c) as indicated in the figure. The triangles are data from SATURNE [28,26], the squares are from ZGS ANL [67], and the circles are from COSY-EDDA [24,25]. The shaded bands illustrate the uncertainty of our calculation. The arrows indicate the squared four-momenta corresponding to the scattering angle $\theta_{c.m.}=90^\circ$.

polarized target where the direction is defined with respect to the proton beam. Extensive measurements of A_{NN} were done at SATURNE [29,30,78] and at COSY-EDDA [79]. The double polarization observable C_{NN} , or spin correlation parameter, was measured [66] at ZGS ANL. Since $A_{NN} = C_{NN}$ due to time reversal invariance, in the following we use always the notation A_{NN} . References to

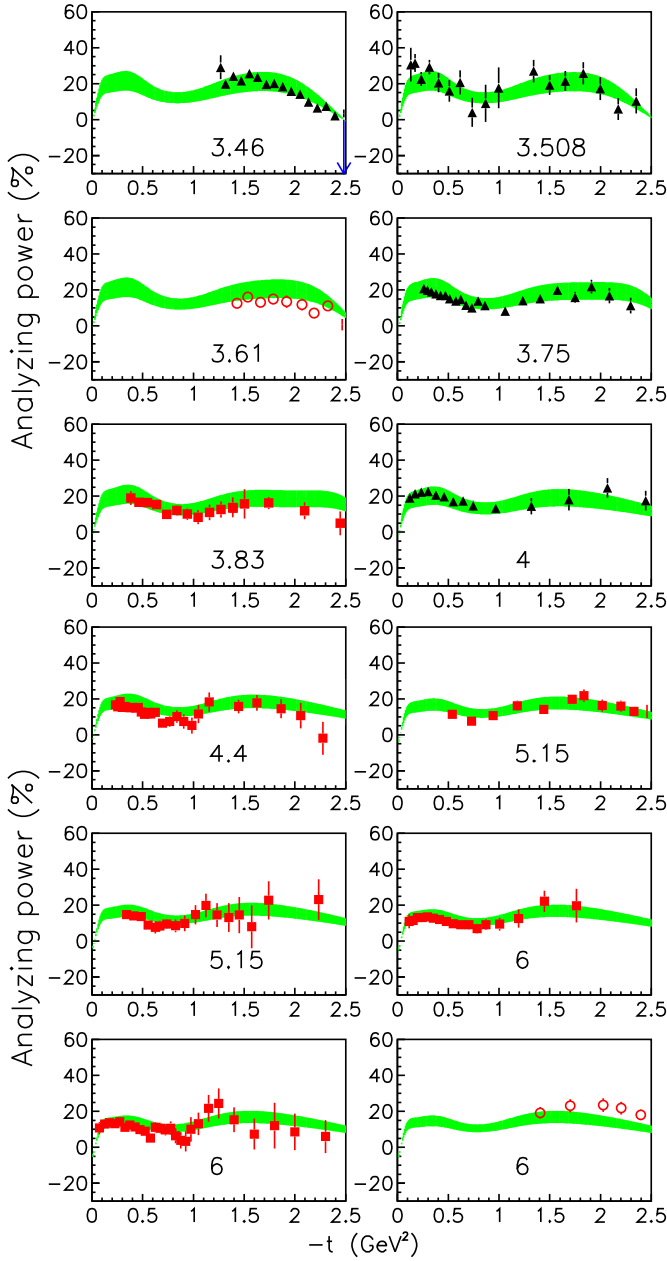


Fig. 10. Analyzing power for pp elastic scattering as a function of the four-momentum transfer squared t for different beam momenta (in GeV/c) as indicated in the figure. The triangles are data from SATURNE [28,26,68], the squares are from ZGS ANL [66,67,70], and the open circles are from CERN PS [69]. The shaded bands illustrate the uncertainty of our calculation. The arrows indicate the squared four-momenta corresponding to the scattering angle $\theta_{c.m.}=90^\circ$.

the data considered in the present work are summarized in Table 5.

Most of the A_{NN} data at beam momenta above 3 GeV/c come from SATURNE. These data are shown by solid triangles in Figs. 12 and 13. Note that at some beam momenta there are two data sets which were actually published in different papers and obviously obtained from dif-

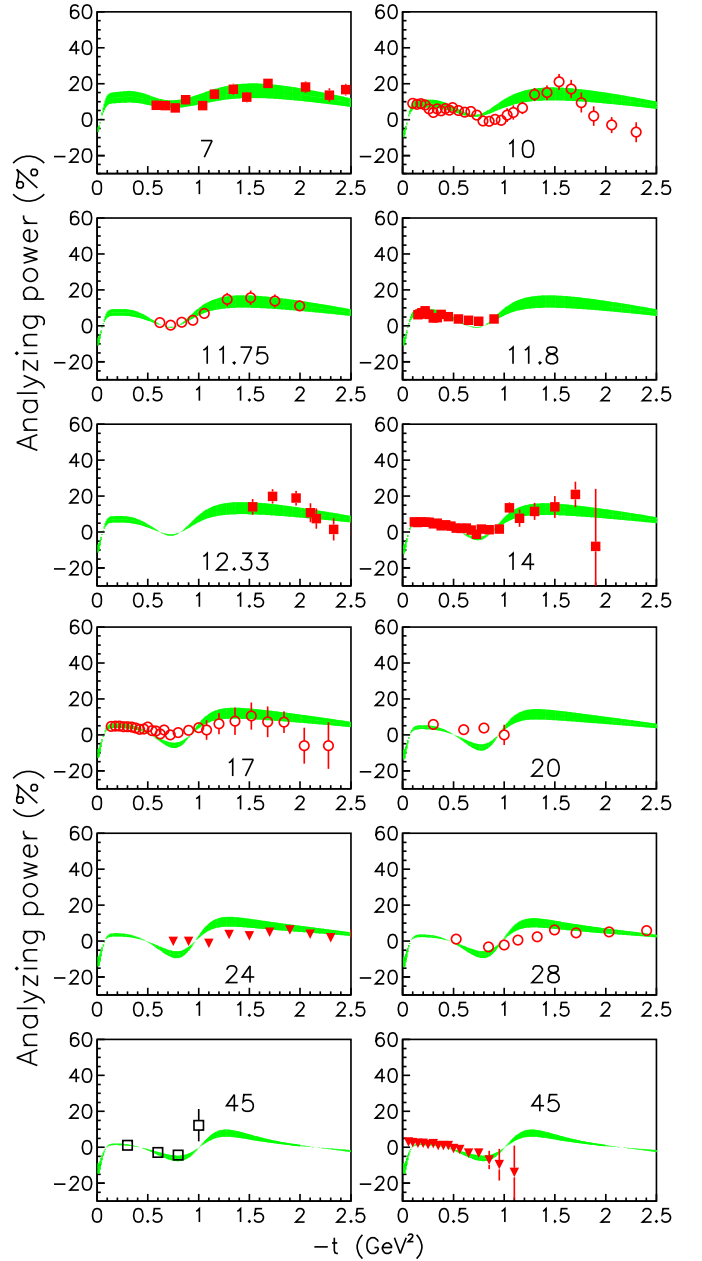


Fig. 11. Analyzing power for pp elastic scattering as a function of the four-momentum transfer squared t for different beam momenta (in GeV/c) as indicated in the figure. The inverse triangles are data from FNAL [76], the squares are from ZGS ANL [70,71,72,73], and the open circles are from CERN PS [74,75]. The shaded bands illustrate the uncertainty of our calculation. The arrows indicate the squared four-momenta corresponding to the scattering angle $\theta_{c.m.}=90^\circ$.

ferent series of measurements, cf. Table 5. Unfortunately, the more recent SATURNE measurement [29,30] does not cover the region of forward angles. In general, the SATURNE data do not indicate any structures. Our Regge model predicts some structure in the t -dependence of the double polarization parameter A_{NN} at $|t| \leq 1 \text{ GeV}^2$, specifically a clear minimum around $|t|=0.5 \text{ GeV}^2$. The COSY-

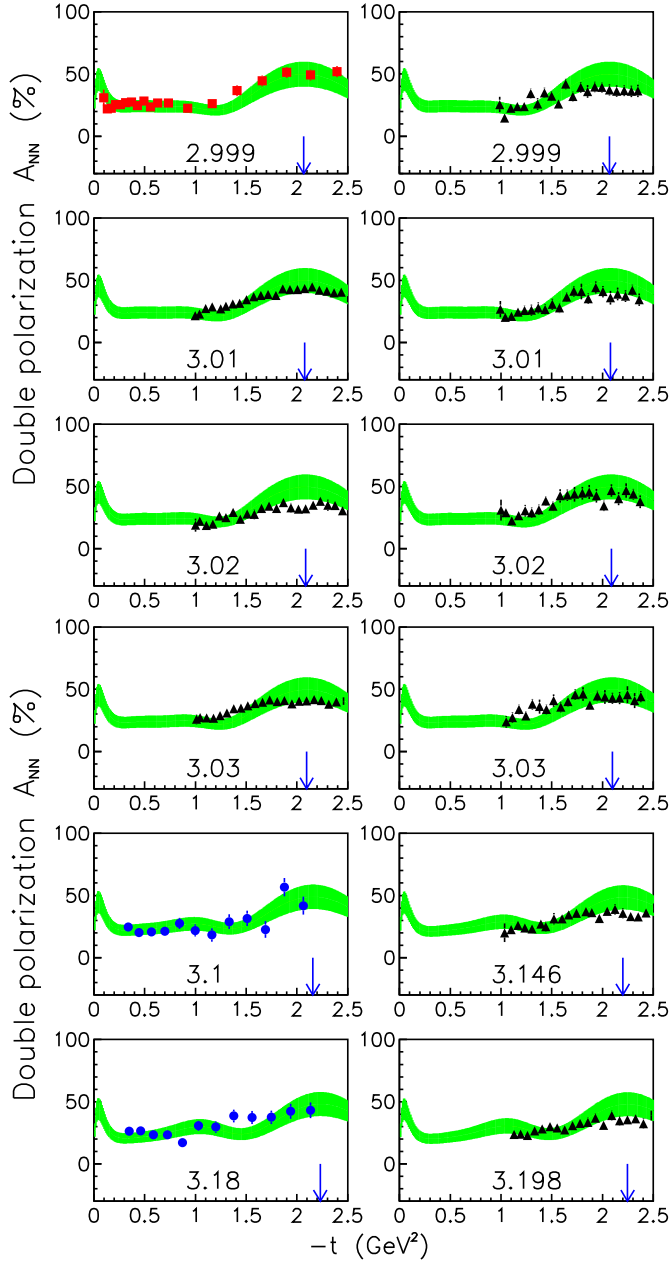


Fig. 12. Double polarization parameter A_{NN} for pp elastic scattering as a function of the four-momentum transfer squared t for different beam momenta (in GeV/c) as indicated in the figure. The triangles are data from SATURNE [29, 30], the squares are from ZGS ANL [66], and the circles are from COSY-EDDA [79]. The shaded bands illustrate the uncertainty of our calculation. The arrows indicate the squared four-momenta corresponding to the scattering angle $\theta_{c.m.}=90^\circ$.

EDDA data [79] at 3.1 GeV/c seem to support such a minimum, though this is not the case for their results at two other momenta.

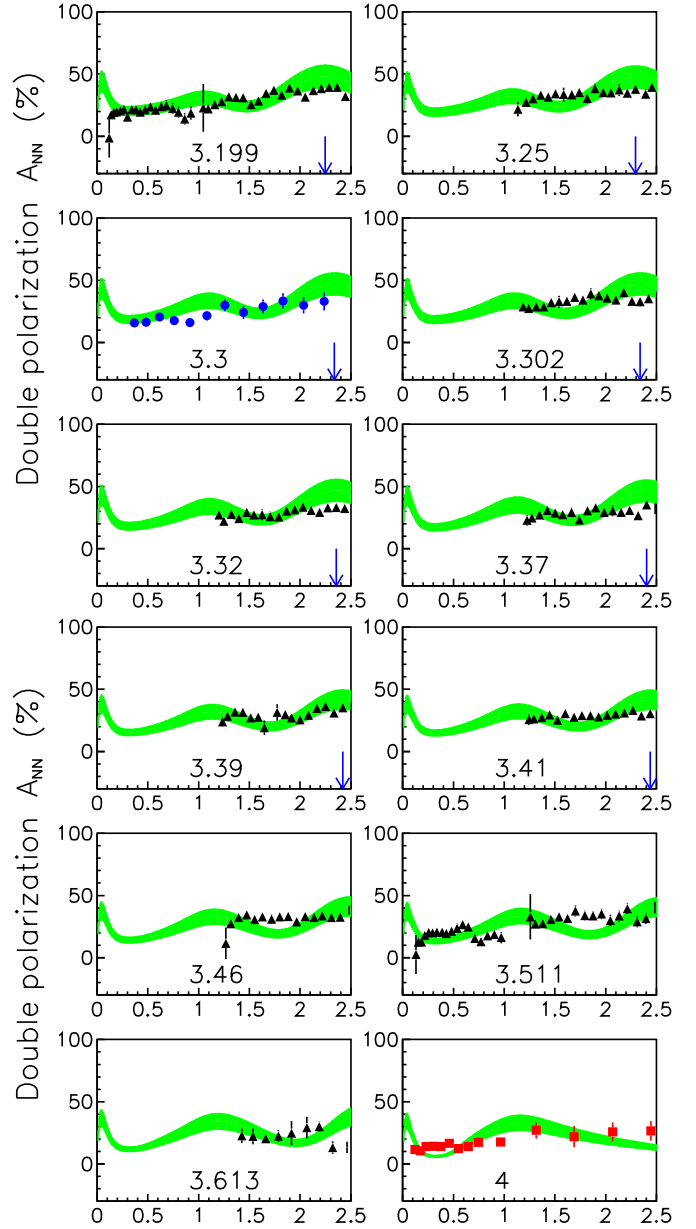


Fig. 13. Double polarization parameter A_{NN} for pp elastic scattering as a function of the four-momentum transfer squared t for different beam momenta (in GeV/c) as indicated in the figure. The triangles are data from SATURNE [29, 30, 78], the squares are from ZGS ANL [66], and the circles are from COSY-EDDA [79]. The shaded bands illustrate the uncertainty of our calculation. The arrows indicate the squared four-momenta corresponding to the scattering angle $\theta_{c.m.}=90^\circ$.

4.4 Total cross sections

The relation between the total pp cross section and the invariant helicity non-flip amplitudes is given by the optical theorem [80],

$$\sigma_{tot} = \frac{\text{Im}[\phi_1(t=0) + \phi_3(t=0)]}{2\sqrt{s^2 - 4sm_N^2}}. \quad (20)$$

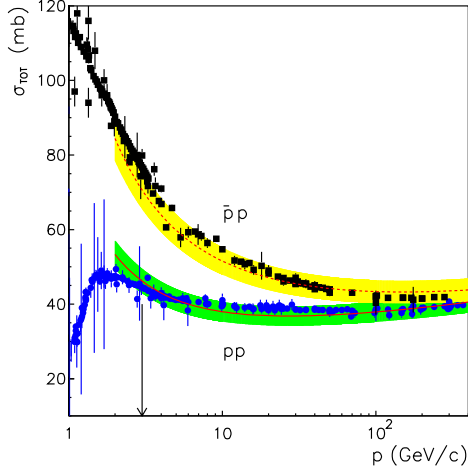


Fig. 14. Total cross sections for the pp and $\bar{p}p$ reactions as a function of the beam momentum. The data are taken from the PDG [32]. The solid and dashed lines show our result obtained via the optical theorem for pp and $\bar{p}p$ scattering, respectively. The shaded band illustrates the uncertainty of our model calculation. The arrow indicates the beam momentum of 3 GeV/c. Only data above that value were included in our fit.

Data on the total pp cross section, taken from the publication of the Particle Data Group [32], are shown in Fig. 14 as a function of the proton beam momentum. Note that in the global fit we included the data available at momenta from 3 to 50 GeV/c. However, as seen in Fig. 14, the total pp cross section can be well described up to proton beam momenta of 400 GeV/c. In fact, the choice of the intercept of the Pomeron contribution, cf. Eq. (13), implies that the pp cross section predicted by our Regge model still remains in line with the data at much higher energies [52]. The arrow in Fig. 14 indicates the beam momentum of 3 GeV/c. As one can see, the total cross section is reasonably well reproduced down to $p \simeq 2$ GeV/c within the indicated uncertainty.

Let us now present our results for the other baryon-baryon reactions involving nucleons and/or antinucleons. Taking into account the isospin structure and the G -parity relations the contributions of the ω , ρ , f_2 , a_2 Regge exchanges and of the Pomeron to the pp , $\bar{p}p$, pn and $\bar{p}n$ scattering amplitudes are given by (see, e.g. [41])

$$\begin{aligned}\phi(pp) &= -\phi_\omega - \phi_\rho + \phi_{f_2} + \phi_{a_2} + \phi_P, \\ \phi(\bar{p}p) &= \phi_\omega + \phi_\rho + \phi_{f_2} + \phi_{a_2} + \phi_P, \\ \phi(pn) &= -\phi_\omega + \phi_\rho + \phi_{f_2} - \phi_{a_2} + \phi_P, \\ \phi(\bar{p}n) &= \phi_\omega - \phi_\rho + \phi_{f_2} - \phi_{a_2} + \phi_P.\end{aligned}\quad (21)$$

Corresponding results for the $\bar{p}p$, pn and $\bar{p}n$ total cross sections can be found in Figs. 14 and 15, together with pertinent data. Obviously, our Regge model yields a good overall description of those three reaction channels too, over practically the whole considered momentum range.

Finally, Fig. 16 shows the ratio of the real-to-imaginary parts of the forward pp and $\bar{p}p$ scattering amplitudes as a function of beam momentum. Again the data are taken from the PDG [32]. The pp data are well described up to

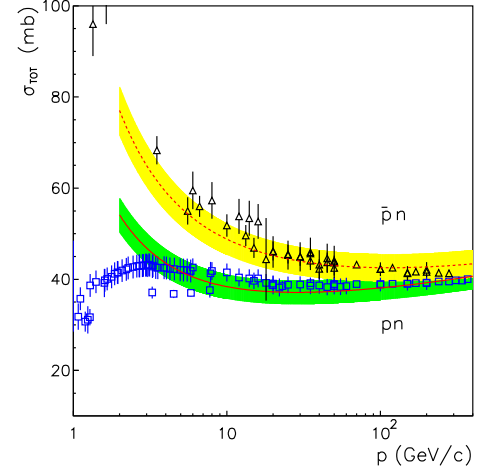


Fig. 15. Total cross sections for the pn and $\bar{p}n$ (c) as a function of the beam momentum shown by the solid and dashed lines, respectively. The data are taken from the PDG [32].

momenta of around 200 GeV/c. In case of $\bar{p}p$ our results seem to overestimate the data somewhat, but one has to keep in mind that the experimental information is fairly poor over the whole considered momentum range.

5 Comparison with results from the GWU partial wave analysis

It is interesting to compare our calculations with the results from partial wave analyses. Among different PWA's the one from the George Washington University [81,82,83] extends up to proton beam momenta of about 3.8 GeV/c.

Since pp elastic scattering is governed by five independent amplitudes a determination of those amplitudes (modulo an overall phase) would require 9 independent observables. When projecting those amplitudes to par-

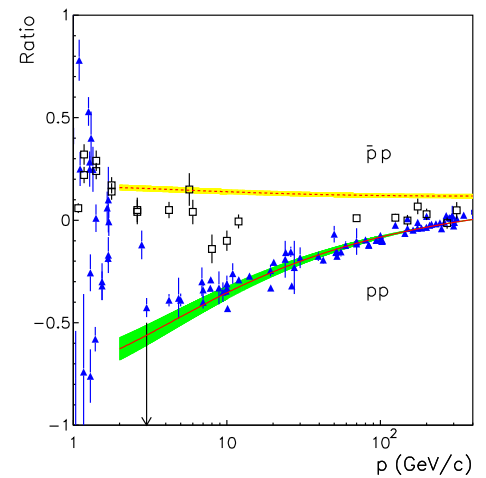


Fig. 16. Ratio of the real-to-imaginary parts of the forward amplitudes for pp (triangles, solid line) and $\bar{p}p$ (squares, dashed line), respectively. The data are taken from the PDG [32].

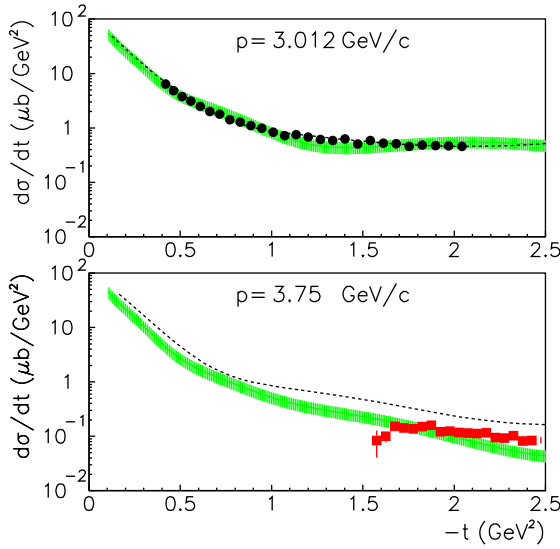


Fig. 17. Differential cross section for pp scattering as a function of the four-momentum transfer squared for the beam momenta of 3.012 GeV/c and 3.75 GeV/c. The circles are data from COSY-EDDA [61], while the squares are the results from ZGS ANL [62,63]. The shaded bands illustrate the uncertainty of our calculation. The dashed lines represent the results from the GWU PWA [82,83].

tial waves one needs to know them over the full angular range. However, the only observables at beam momenta above 3 GeV/c, where more or less full information on their angular dependence is available, are differential cross sections, analyzing powers (polarizations) and the double polarization parameter $A_{NN} = C_{NN}$. There are some data on other polarization observables, though they are available only for a few beam momenta above 3 GeV/c. Therefore, obtaining a PWA solution at $p \geq 3$ GeV/c that is unique and represents the experimental results in an appropriate way is a challenging task. Indeed the recent data from COSY-EDDA and SATURNE were quite instrumental to improve the GWU PWA [81,82,83], available at the SAID [84,85] webpage.

Since the GWU PWA and our Regge analysis overlap within the momentum range of 3 to 3.8 GeV/c we show here selected results close to these two momenta for a comparison. For illustration we also include the experimental results.

The differential cross sections for pp scattering at beam momenta of 3.012 and 3.75 GeV/c are displayed in Fig. 17. The data are from measurements at COSY-EDDA [61] and at ZGS ANL [62,63]. Again the shaded bands indicate the uncertainty of our solution. The dashed lines are results based on the GWU PWA [82,83]. At the lower beam momentum our Regge model as well as the GWU PWA are in line with the experimental information while at the higher momentum the GWU PWA overestimates the data somewhat.

Fig. 18 depicts the analyzing powers for pp scattering at beam momenta of 3.01 and 3.75 GeV/c. The data are from measurements at SATURNE [27] and at ZGS ANL [67]. At the beam momentum of 3.01 GeV/c our

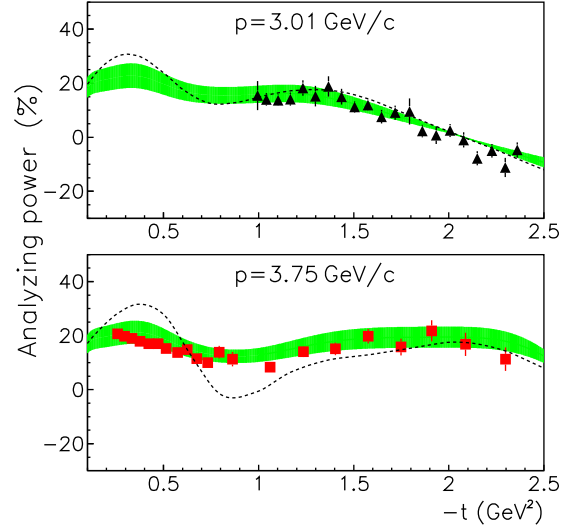


Fig. 18. Analyzing power for pp scattering as a function of the four-momentum transfer squared for the beam momenta of 3.01 GeV/c and 3.75 GeV/c. The triangles are data from SATURNE [27], while the squares are the results from ZGS ANL [67]. The shaded bands illustrate the uncertainty of our calculation. The dashed lines represents the results from the GWU PWA [82,83].

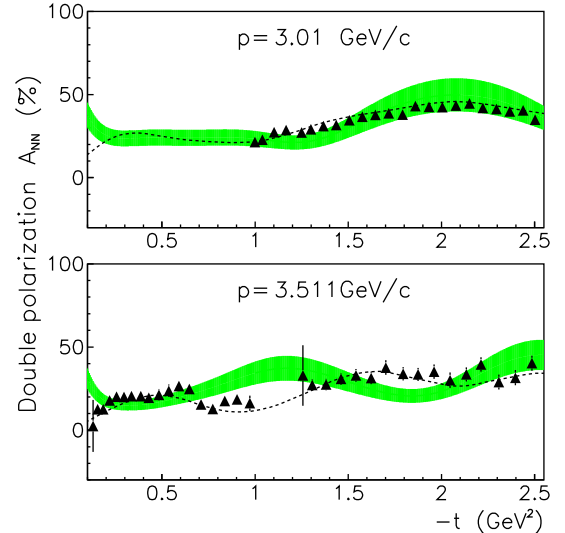


Fig. 19. Double polarization parameter A_{NN} for pp scattering as a function of the four-momentum transfer squared for the beam momenta of 3.01 GeV/c and 3.511 GeV/c. The triangles are data from SATURNE [30,78]. The shaded bands illustrate the uncertainty of our calculation. The dashed lines represents the results from the GWU PWA [82,83].

Regge model as well as the GWU PWA describe the data. At the higher momentum the GWU PWA already fails to reproduce the data, while our solution is still in rather good agreement with the experimental information.

Fig. 19 shows the double polarization parameter A_{NN} at beam momenta of 3.01 and 3.511 GeV/c. The data are from measurements at SATURNE [30,78]. Here the Regge

approach agrees with both data and the GWU PWA for $|t| < 0.5 \text{ GeV}^2$ for the beam momentum 3.511 GeV/c.

6 Summary

We performed a systematic analysis of pp scattering at beam momenta from 3 GeV/c up to 50 GeV/c utilizing the Regge formalism. Experimental results on differential cross sections, analyzing powers, and double polarization parameters available from recent measurements at COSY-EDDA, SATURNE as well as data collected previously at ZGS ANL allow to construct the Regge amplitudes for pp scattering with reasonable accuracy. For momenta below 4 GeV/c there are no precise data at forward direction, i.e. at scattering angles below 30° in the center-of-mass system. Therefore, the amplitudes cannot be fixed in a unique way at these angles. Usually, the Regge model works rather well at small four-momentum transfer squared or forward angles and it would be crucial to collect new data in this kinematical region. We expect that further progress in the analysis of pp scattering will become possible with forthcoming data from the ANKE COSY Collaboration [31], which will cover the momentum range analyzed here but will include angles in forward direction.

We are indebted to N.N. Nikolaev for instructive discussions. This work is partially supported by the Helmholtz Association through funds provided to the virtual institute “Spin and strong QCD” (VH-VI-231), by the EU Integrated Infrastructure Initiative HadronPhysics2 Project (WP4 QCDnet) and by DFG (SFB/TR 16, “Subnuclear Structure of Matter”). This work was also supported in part by U.S. DOE Contract No. DE-AC05-06OR23177, under which Jefferson Science Associates, LLC, operates Jefferson Lab. A.S. acknowledges support by the JLab grant SURA-06-C0452 and the COSY FFE grant No. 41760632 (COSY-085).

References

1. W.M. Kloet and R.R. Silbar, Nucl. Phys. A **338**, 281 (1980).
2. W.M. Kloet and R.R. Silbar, Nucl. Phys. A **364**, 346 (1981).
3. J. Dubach, W.M. Kloet and R.R. Silbar, Nucl. Phys. A **466**, 573 (1982).
4. T.S.H. Lee, Phys. Rev. C **29**, 195 (1984).
5. E.E. van Faassen and J.A. Tjon, Phys. Rev. C **30**, 285 (1984).
6. E.E. van Faassen and J.A. Tjon, Phys. Rev. C **33**, 2105 (1986).
7. B. ter Haar and R. Malfiet, Phys. Rept. **149**, 207 (1987).
8. R. Machleidt, K. Holinde and C. Elster, Phys. Rept. **149**, 1 (1987).
9. J. Haidenbauer, K. Holinde and M. B. Johnson, Phys. Rev. C **48**, 2190 (1993).
10. R. Machleidt, Phys. Rev. C **63**, 024001 (2001).
11. K. O. Eyster, R. Machleidt and W. Scobel, Eur. Phys. J. A **22**, 105 (2004) [arXiv:nucl-th/0311002].
12. A. Pricking, C. Elster, A. Gårdestig and F. Hinterberger, arXiv:0708.3692 [nucl-th].
13. R. Machleidt and I. Slaus, J. Phys. G **27**, R69 (2001).
14. H.V. von Geramb, K.A. Amos, H. Labes and M. Sander, Phys. Rev. C **58**, 1948 (1998).
15. V.G. Neudachin, N.P. Yudin, I.T. Obukhovskiy and Yu.L. Dorodnykh, Phys. Rev. C **43**, 2499 (1991).
16. A. Funk, H.V. von Geramb and K.A. Amos, Phys. Rev. C **64**, 054003 (2001).
17. V.A. Knyr, V.G. Neudachin and N.A. Khokhlov, Phys. Atom. Nucl. **69**, 2034 (2006).
18. N.H. Buttigieg, B.Z. Kopeliovich, E. Leader, J. Soffer and T.L. Trueman, Phys. Rev. D **59**, 114010 (1999).
19. N.I. Kochelev, D.-P. Min, Y. Oh, V. Vento and A.V. Vinnikov, Phys. Rev. D **61**, 094008 (2000).
20. D. Kharzeev and E. Levin, Nucl. Phys. B **578**, 351 (2000).
21. A. Donnachie and P.V. Landshoff, Phys. Lett. B **518**, 63 (2001).
22. A. Donnachie and P.V. Landshoff, Phys. Lett. B **595**, 393 (2004).
23. J. R. Cudell, A. Lengyel and E. Martynov, Phys. Rev. D **73**, 034008 (2006).
24. M. Altmeier *et al.*, Phys. Rev. Lett. **85**, 1819 (2000).
25. M. Altmeier *et al.*, Eur. Phys. J. A **23**, 351 (2005).
26. F. Perrot *et al.*, Nucl. Phys. B **294**, 1001 (1987).
27. C.E. Allgower *et al.*, Phys. Rev. C **60**, 054001 (1999).
28. C.E. Allgower *et al.*, Phys. Rev. C **60**, 054002 (1999).
29. C.E. Allgower *et al.*, Phys. Rev. C **62**, 064001 (2000).
30. C.E. Allgower *et al.*, Phys. Rev. C **64**, 034003 (2001).
31. D. Chiladze *et al.* (ANKE Collaboration), COSY Proposal No. 200 (2009).
32. C. Amsler *et al.* (Particle Data Group), Phys. Lett. B **667**, 1 (2008).
33. A. Sibirtsev, J. Haidenbauer, S. Krewald, T.S.H. Lee, Ulf-G. Meißner and A.W. Thomas, Eur. Phys. J. A **34**, 49 (2007).
34. A. Sibirtsev, J. Haidenbauer, F. Huang, S. Krewald and U.-G. Meißner, Eur. Phys. J. A **40**, 65 (2009).
35. F. Huang, A. Sibirtsev, S. Krewald, C. Hanhart, J. Haidenbauer and Ulf-G. Meißner, Eur. Phys. J. A **40**, 77 (2009).
36. A. Sibirtsev, J. Haidenbauer, S. Krewald, U.-G. Meißner and A.W. Thomas, Eur. Phys. J. A **41**, 71 (2009).
37. F. Huang, A. Sibirtsev, J. Haidenbauer, S. Krewald, and Ulf-G. Meißner, Eur. Phys. J. A **44**, 81 (2010).
38. F. Arbab and J.W. Dash, Phys. Rev. **163**, 1603 (1967).
39. W. Rarita, R.J. Riddell, C.B. Chiu and R.J.N. Phillips, Phys. Rev. **165**, 1615 (1968).
40. J.L. Cudell *et al.*, Phys. Rev. D **65**, 074024 (2002).
41. J.R. Pelaez, PoS HEP2005, 46 (2006).
42. M. Jacob and G.C. Wick, Ann. Phys. **7**, 404 (1959).
43. J. Bystricky, F. Lehar and P. Winternitz, J. Phys. (France) **39**, 1 (1978).
44. M.L. Goldberger, M.T. Grisaru, S.W. MacDowell and D.Y. Wong, Phys. Rev. **120**, 2250 (1960).
45. A. C. Irving and R. P. Worden, Phys. Rept. **34**, 117 (1977).
46. P.D.B. Collins, *An Introduction to Regge Theory and High Energy Physics*, Cambridge University, Cambridge, England (1977) 275.
47. P.D.B. Collins and A.D. Martin, Rept. Prog. Phys. **45**, 335 (1982).
48. D.H. Sharp and W.G. Wagner, Phys. Rev. **131**, 2226 (1963).
49. C. Itzykson and M. Jacob, Nuovo Cim. **28**, 250 (1963).

50. A. Donnachie and P.V. Landshoff, Nucl. Phys. B **231**, 189 (1984).
51. A. Donnachie and P.V. Landshoff, Nucl. Phys. B **267**, 690 (1986).
52. A. Donnachie and P.V. Landshoff, Phys. Lett. B **296**, 227 (1992).
53. A.V. Anisovich, V.V. Anisovich and A.V. Sarantsev, Phys. Rev. D **62**, 051502 (2000).
54. A. Sibirtsev, K. Tsushima and S. Krewald, Phys. Rev. C **67**, 055201 (2003).
55. C. Avilez, G. Cocho, and M. Moreno, Phys. Rev. D **24**, 6344 (1981).
56. R.F. Avila, P. Gauron and B. Nicolescu, Eur. Phys. J. C **49**, 581 (2007).
57. E. Martynov, Phys. Rev. D **76**, 07430 (2007).
58. A.D. Krisch, arXiv:1001.0790 [hep-ex].
59. T.E.O. Ericson *et al.*, Phys. Rev. Lett. **75**, 1046 (1995).
60. W. Rarita and V.L. Teplitz, Phys. Rev. Lett. **12**, 206 (1964).
61. D. Albers *et al.*, Eur. Phys. J. A **22**, 125 (2004).
62. K.A. Jenkins *et al.*, Phys. Rev. Lett. **40**, 425 (1978).
63. K.A. Jenkins *et al.*, Phys. Rev. D **21**, 2445 (1980).
64. see, e.g., B. Holzenkamp, K. Holinde, J. Speth, Nucl. Phys. A **500**, 485 (1989).
65. R.C. Kammerud *et al.*, Phys. Rev. D **4**, 1309 (1971).
66. D. Miller *et al.*, Phys. Rev. D **16**, 2016 (1977).
67. J.H. Parry *et al.*, Phys. Rev. D **8**, 45 (1973).
68. J. Deregel *et al.*, Nucl. Phys. B **103**, 269 (1976).
69. M. Borghini *et al.*, Phys. Lett. **31** B, 405 (1970).
70. G.W. Abshire *et al.*, Phys. Rev. Lett. **32**, 1261 (1974).
71. S.L. Linn *et al.*, Phys. Rev. D **26**, 550 (1982).
72. K. Abe *et al.*, Phys. Lett. B **63**, 239 (1976).
73. S.L. Kramer *et al.*, Phys. Rev. D **17**, 1709 (1978).
74. M. Borghini *et al.*, Phys. Lett. B **36**, 501 (1971).
75. J. Antille *et al.*, Nucl. Phys. B **185**, 1 (1981).
76. M. Corcoran *et al.*, Phys. Rev. D **22**, 2624 (1980).
77. P.H. Hansen *et al.*, Phys. Rev. Lett. **50**, 802 (1983).
78. F. Lehar *et al.*, Nucl. Phys. B **294**, 1013 (1987).
79. F. Bauer *et al.*, Phys. Rev. C **71**, 054002 (2005).
80. E. Byckling and K. Kajantie, Particle Kinematics (Wiley and Sons, New York, 1973).
81. R.A. Arndt, C.H. Oh, I.I. Strakovsky, R.L. Workman and F. Dohrmann, Phys. Rev. C **56**, 3005 (1997).
82. R.A. Arndt, I.I. Strakovsky and R.L. Workman, Phys. Rev. C **62**, 034005 (2000).
83. R.A. Arndt, W.J. Briscoe, I.I. Strakovsky, and R.L. Workman, Rev. C **76**, 025209 (2007).
84. R.A. Arndt, L.D. Roper, R.A. Bryan, R.B. Clark, B.J. VerWest, and P. Signell, Phys. Rev. D **28**, 97 (1983).
85. R.A. Arndt, I.I. Strakovsky and R.L. Workman, Phys. Rev. C **50**, 2731 (1994).
86. K.J. Foley *et al.*, Phys. Rev. Lett. **11**, 425 (1963).
87. J. Orear *et al.*, Phys. Rev. **152**, 1162 (1966).
88. D. Harting *et al.*, Nuovo Cim. **38**, 60 (1965).
89. K.J. Foley *et al.*, Phys. Rev. Lett. **15**, 45 (1965).
90. A.N. Diddens *et al.*, Phys. Rev. Lett. **9**, 108 (1962).
91. C. Bruneton *et al.*, Nucl. Phys. B **124**, 391 (1977).
92. Z. Asad *et al.*, Nucl. Phys. B **255**, 273 (1985).
93. P. Jenni *et al.*, Nucl. Phys. B **129**, 232 (1977).
94. J.V. Allaby *et al.*, Nucl. Phys. B **52**, 316 (1973).
95. G.G. Beznogikh *et al.*, Nucl. Phys. B **54**, 78 (1973).
96. I.M. Geshkov, N.L. Ikov, P.K. Markov, R.K. Trayanov, Phys. Rev. D **13**, 1846 (1976).

7 Appendix

In this appendix we summarize information on the proton-proton scattering data analyzed in the present work.

Table 2. References to data on differential cross sections for elastic pp scattering analyzed in the present work. Here p is the proton beam momentum in the laboratory system, and t_{min} and t_{max} denote the minimal and maximal four-momentum transfer squared, respectively.

p (GeV/c)	t_{min} GeV ²	t_{max} GeV ²	Experiment	Ref.
3.012	-2.043	-0.419	COSY-EDDA	[61]
3.017	-2.075	-1.225	ZGS ANL	[62,63]
3.036	-2.064	-0.423	COSY-EDDA	[61]
3.062	-2.087	-0.428	COSY-EDDA	[61]
3.087	-2.109	-0.432	COSY-EDDA	[61]
3.095	-2.125	-1.225	ZGS ANL	[62,63]
3.112	-2.131	-0.437	COSY-EDDA	[61]
3.137	-2.153	-0.441	COSY-EDDA	[61]
3.150	-2.175	-1.375	ZGS ANL	[62,63]
3.162	-2.175	-0.446	COSY-EDDA	[61]
3.187	-2.197	-0.450	COSY-EDDA	[61]
3.205	-2.225	-1.325	ZGS ANL	[62,63]
3.212	-2.219	-0.455	COSY-EDDA	[61]
3.237	-2.242	-0.459	COSY-EDDA	[61]
3.262	-2.264	-0.513	COSY-EDDA	[61]
3.266	-2.275	-1.275	ZGS ANL	[62,63]
3.287	-2.286	-0.518	COSY-EDDA	[61]
3.312	-2.308	-0.523	COSY-EDDA	[61]
3.337	-2.330	-0.529	COSY-EDDA	[61]
3.350	-2.325	-1.325	ZGS ANL	[62,63]
3.362	-2.352	-0.534	COSY-EDDA	[61]
3.388	-2.375	-0.539	COSY-EDDA	[61]
3.410	-2.350	-1.300	ZGS ANL	[62,63]
3.469	-2.399	-1.450	ZGS ANL	[62,63]
3.499	-2.501	-0.379	ZGS ANL	[65]
3.530	-2.525	-1.375	ZGS ANL	[62,63]
3.621	-2.625	-1.475	ZGS ANL	[62,63]
3.686	-2.675	-1.575	ZGS ANL	[62,63]
3.750	-2.725	-1.575	ZGS ANL	[62,63]
3.843	-2.850	-1.350	ZGS ANL	[62,63]
3.942	-2.850	-1.450	ZGS ANL	[62,63]
4.013	-2.850	-1.550	ZGS ANL	[62,63]
4.082	-2.950	-1.750	ZGS ANL	[62,63]
4.151	-3.050	-1.650	ZGS ANL	[62,63]
4.2	-0.0188	-1.6·10 ⁻³	CERN PS	[93]
4.258	-3.150	-1.750	ZGS ANL	[62,63]
4.334	-3.150	-1.850	ZGS ANL	[62,63]
4.409	-3.250	-1.950	ZGS ANL	[62,63]
4.483	-3.250	-1.650	ZGS ANL	[62,63]
4.559	-3.450	-1.750	ZGS ANL	[62,63]
4.681	-3.550	-1.950	ZGS ANL	[62,63]
6.800	-0.863	-0.023	AGS BNL	[86]

Table 3. References to data on differential cross sections for elastic pp scattering analyzed in the present work. Here p is the proton beam momentum in the laboratory system, and t_{min} and t_{max} denote the minimal and maximal four-momentum transfer squared, respectively.

p (GeV/c)	t_{min} GeV ²	t_{max} GeV ²	Experiment	Ref.
7.0	-5.85·10 ⁻²	-1.41·10 ⁻³	CERN PS	[93]
8.000	-3.500	-1.740	AGS BNL	[87]
8.500	-1.050	-0.130	CERN PS	[88]
8.800	-0.916	-0.039	AGS BNL	[86]
10.0	-9.72·10 ⁻²	-1.8·10 ⁻³	CERN PS	[93]
10.0	-2.05	-0.135	CERN PS	[94]
10.800	-0.824	-0.058	AGS BNL	[86]
10.940	-0.891	-0.200	AGS BNL	[89]
12.000	-2.500	-1.200	AGS BNL	[87]
12.0	-2.74	-0.104	CERN PS	[94]
12.100	-0.342	-0.011	CERN PS	[90]
12.400	-2.000	-0.130	CERN PS	[88]
12.800	-0.856	-0.049	AGS BNL	[86]
13.16	-0.104	-9.2·10 ⁻³	CERN PS	[95]
14.2	-3.54	-0.273	CERN PS	[94]
14.800	-0.781	-0.066	AGS BNL	[86]
14.930	-0.736	-0.216	AGS BNL	[89]
15.500	-0.563	-0.019	CERN PS	[90]
15.52	-0.107	-8.9·10 ⁻³	CERN PS	[95]
16.700	-0.698	-0.042	AGS BNL	[86]
18.400	-3.600	-0.190	CERN PS	[88]
18.600	-0.794	-0.036	CERN PS	[90]
19.600	-0.811	-0.115	AGS BNL	[86]
19.840	-0.787	-0.230	AGS BNL	[89]
21.400	-1.055	-0.032	CERN PS	[90]
21.880	-0.807	-0.235	AGS BNL	[89]
24.0	-6.72	-0.0828	CERN PS	[94]
24.56	-0.111	-1.1·10 ⁻²	CERN PS	[95]
24.630	-0.748	-0.254	AGS BNL	[89]
26.200	-1.042	-0.064	CERN PS	[90]
30.00	-0.119	-2.7·10 ⁻³	CERN PS	[96]
30.45	-0.113	-1.1·10 ⁻²	CERN PS	[95]
44.500	-2.003	-0.161	Serpukhov	[91]
45.17	-0.115	-1.1·10 ⁻²	CERN PS	[95]
50.000	-4.00	-0.8	CERN SPS	[92]

Table 4. References to data on analyzing powers A and polarizations P for elastic pp scattering ($A=P$) analyzed in the present work. Here p is the proton beam momentum in the laboratory system, and t_{min} and t_{max} denote the minimal and maximal four-momentum transfer squared, respectively.

p (GeV/c)	t_{min} GeV ²	t_{max} GeV ²	Experiment	Ref.
2.999	-2.349	-0.988	SATURNE	[27]
3.00	-2.803	-0.082	ZGS ANL	[66]
3.01	-2.359	-0.994	SATURNE	[27]
3.015	-2.009	-0.316	COSY-EDDA	[24, 25]
3.021	-2.37	-1.0	SATURNE	[27]
3.031	-2.38	-1.05	SATURNE	[27]
3.045	-2.035	-0.320	COSY-EDDA	[24, 25]
3.075	-2.061	-0.325	COSY-EDDA	[24, 25]
3.105	-2.087	-0.329	COSY-EDDA	[24, 25]
3.135	-2.113	-0.333	COSY-EDDA	[24, 25]
3.146	-2.716	-1.35	SATURNE	[28]
3.165	-2.139	-0.337	COSY-EDDA	[24, 25]
3.195	-2.165	-0.341	COSY-EDDA	[24, 25]
3.196	-2.4	-0.156	SATURNE	[26]
3.198	-2.778	-1.129	SATURNE	[28]
3.225	-2.191	-0.345	COSY-EDDA	[24, 25]
3.25	-2.604	-0.232	ZGS ANL	[67]
3.251	-2.844	-1.137	SATURNE	[28]
3.29	-2.953	-1.187	SATURNE	[28]
3.3	-2.257	-0.355	COSY-EDDA	[24, 25]
3.32	-2.979	-1.2	SATURNE	[28]
3.37	-3.043	-1.228	SATURNE	[28]
3.39	-3.054	-1.233	SATURNE	[28]
3.41	-3.081	-1.243	SATURNE	[28]
3.46	-3.137	-1.268	SATURNE	[28]
3.508	-3.052	-0.129	SATURNE	[26]
3.61	-3.263	-1.428	SATURNE	[28]
3.75	-2.298	-0.258	ZGS ANL	[67]
3.83	-2.783	-0.383	SATURNE	[68]
4.00	-2.989	-0.097	ZGS ANL	[66]
4.40	-2.96	-0.233	ZGS ANL	[67]
5.15	-4.055	-0.341	ZGS ANL	[67]
5.15	-4.031	-0.54	ZGS ANL	[70]
6.00	-1.926	-0.098	ZGS ANL	[66]
6.00	-2.5	-0.05	CERN PS	[69]
6.00	-4.62	-1.40	ZGS ANL	[71]
7.0	-5.245	-0.582	ZGS ANL	[70]
10.0	-2.9	-0.08	CERN PS	[74]
11.75	-2.509	-0.618	ZGS ANL	[72]
11.8	-0.9	-0.15	ZGS ANL	[73]
12.33	-6.191	-1.531	ZGS ANL	[70]
14.0	-2.0	-0.1	CERN PS	[74]
17.0	-2.64	-0.17	CERN PS	[74]
20.0	-1.0	-0.3	FNAL	[76]
24.0	-5.0	-0.7	CERN PS	[75]
28.0	-2.997	-0.525	AGS BNL	[77]
45.0	-1.0	-0.3	FNAL	[76]

Table 5. References to data on the double polarization parameters A_{NN} and C_{NN} , ($A_{NN}=C_{NN}$) for elastic pp scattering analyzed in the present work. Here p is the proton beam momentum in the laboratory system, and t_{min} and t_{max} denote the minimal and maximal four-momentum transfer squared, respectively.

p (GeV/c)	t_{min} GeV ²	t_{max} GeV ²	Experiment	Ref.
2.999	-2.672	-0.097	ZGS ANL	[66]
2.999	-2.348	-0.987	SATURNE	[29]
3.010	-2.502	-0.998	SATURNE	[30]
3.010	-2.360	-0.992	SATURNE	[29]
3.020	-2.563	-1.002	SATURNE	[30]
3.020	-2.370	-0.999	SATURNE	[29]
3.030	-2.574	-1.010	SATURNE	[30]
3.030	-2.376	-1.051	SATURNE	[29]
3.100	-2.063	-0.338	COSY-EDDA	[79]
3.146	-2.713	-1.034	SATURNE	[30]
3.180	-2.133	-0.349	COSY-EDDA	[79]
3.198	-2.778	-1.130	SATURNE	[30]
3.199	-2.513	-0.120	SATURNE	[78]
3.250	-2.844	-1.136	SATURNE	[30]
3.300	-2.235	-0.366	COSY-EDDA	[79]
3.302	-2.954	-1.188	SATURNE	[30]
3.320	-2.974	-1.200	SATURNE	[30]
3.370	-3.035	-1.226	SATURNE	[30]
3.3900	-3.058	-1.235	SATURNE	[30]
3.4100	-3.085	-1.245	SATURNE	[30]
3.4600	-3.138	-1.268	SATURNE	[30]
3.5110	-3.033	-0.131	SATURNE	[78]
3.6130	-3.260	-1.427	SATURNE	[30]
4.0	-2.803	-0.120	ZGS ANL	[66]